



N-doped ZnO/graphene oxide: a photostable photocatalyst for improved mineralization and photodegradation of organic dye under visible light

C. N. Peter¹ · William W. Anku¹ · Rama Sharma² · Girish M. Joshi³ · Sudheesh K. Shukla^{1,4} · Penny P. Govender¹

Received: 29 January 2018 / Revised: 16 April 2018 / Accepted: 20 April 2018 / Published online: 5 May 2018
© Springer-Verlag GmbH Germany, part of Springer Nature 2018

Abstract

This research work focused on the synthesis of visible light-active ZnO photocatalyst through modification with nitrogen and graphene oxide, followed by its application towards the degradation of brilliant smart green (BG) dye. The characterization of the synthesized photocatalysts was done using optical approaches such as X-ray diffraction (XRD), Fourier transform infrared (FTIR), transmission electron microscopy (TEM), UV–vis absorption, and diffuse reflectance spectra (UV–vis DRS). N-ZnO-GO (NZGO-1, NZGO-2, and NZGO-3) composites show a higher photocatalytic activity in degrading BG dye in water compared to ZnO and N-ZnO nanoparticles. The composite NZGO-1 achieved 100% degradation and 80% mineralization of BG within 90 min of irradiation. The results also showed the degradation of BG using NZGO-1 occurs faster in basic medium (pH 9) compared to acidic medium. Photostability test of NZGO-1 analyzed after three cycles of exposure gave 94% degradation of BG which implies that the composite is also highly stable and can be recovered and reused. This study further highlighted that the modifications made on ZnO were positive by increasing its light absorption capability into the visible region and thus drastically improved its photocatalytic activities under visible light.

Keywords Photocatalyst · Dye degradation · ZnO nanoparticles · Brilliant green · Mineralization · Photocatalytic reaction · Visible light · Wastewater treatment

C. N. Peter and William W. Anku have the same contribution to the preparation of this manuscript.

Highlights

- In this work, the characterization of the synthesized photocatalyst affirms a reduction in band gap and suppression of electron-hole recombination rate of ZnO after modifications with nitrogen and graphene oxide.
- Approximately 99% degradation of brilliant green dye in water under simulated solar light together with 80% mineralization was achieved within 90 min of irradiation.
- This work investigated the effect of some important parameters in the disposal of wastewater such as pH and the risk of secondary pollutants on using the synthesized photocatalyst in regard to wastewater remediation.
- This work is expected to draw attention of researchers interested in environmental chemistry and biology, environments' pollution control fate of pollutants in the environment, organic compounds in the environment, atmospheric pollutants, etc.

✉ Sudheesh K. Shukla
sudheeshkshukla@gmail.com

✉ Penny P. Govender
pennyg@uj.ac.za

² Department of Agriculture Science, AKS University, Satna, Madhya Pradesh 485001, India

³ Polymer Nanocomposite Laboratory, Center for Crystal Growth, VIT University, Vellore, TN 632014, India

¹ Department of Applied Chemistry, Doornfontein Campus 2028, University of Johannesburg, Johannesburg, South Africa

⁴ Present address: Department of Biomedical Engineering, Ben-Gurion University, 8410501 Beer Sheva, Israel

Introduction

Although the Earth's surface is covered with a huge amount of water (~71%), only about 0.3% is fresh and accessible to human beings. The rest, 99.7% fresh water, is trapped in the ice caps, soil, and in the atmosphere [1], and even the 0.3% accessible water is unattainable by humans [2]. Available fresh water for human consumption comes from lakes, ponds, reservoirs, streams, and rivers, hence maintaining these water bodies for use is a cause for concern for humanity. Dyes are the most important raw materials used in some of the industries which include paint, plastic, paper, pharmaceutical, textile, cosmetics, and food [3]. Wastewater from these industries usually contains dye residues which are not readily degradable. Wastewater containing these dye residues creates negative effects on the environment especially when they enter into the water bodies. Firstly, due to their color, they hinder the penetration of light into water bodies and therefore affecting the photosynthesis of aquatic systems [4]. Apart from the effect of their color, the effect of dyes on human health is also detrimental. The end products of dyes affect the formation of hemoglobin, skin, and lung [5]. Also, some of these dyes are carcinogenic and may cause dermatitis, allergies, and skin irritation [6]. Hence, it is of utmost importance to properly treat dye-contaminated wastewater before discharging into the environment.

Several conventional techniques have been used in remediation of wastewater problems caused by dye residues. The well-known techniques to flush out this issue include adsorption, reverse osmosis, electrodialysis, coagulation/flocculation, oxidation, irradiation, and aerobic and anaerobic microbial methods of degradation [7]. But, these conventional methods have shown some drawbacks such as incomplete treatment leading to the production of secondary pollutants (e.g., production of trihalomethanes which are carcinogenic, by the reaction of chlorine gas with some of the organic substances found in natural water during the chlorination process) [8], waste management arising from the non-biodegradability of most of the dyes, and high cost of operation [9].

Treatment of wastewater from dye-utilizing industries does not only rely on removal of the color but also on mineralization and degradation of the dye compounds. Advanced oxidation methods have proven to be more efficient because of their pollutant degradability capabilities [10]. The use of semiconductors as photocatalysts [11] is common and well known in advanced oxidation approaches for dye removal. ZnO semiconductors have shown to be effective when compared to other semiconductors used as photocatalysts and have been studied extensively due to its interesting features like wide band gap, weak toxicity, high electron mobility, and strong oxidizing power [12]. However, using ZnO as a photocatalyst exhibits some drawbacks which include its wide band gap (~3.3 eV) (this restricts its application in the UV range that is

only ~5% of visible radiation), the low surface area of the bulk form, and high rate at which the photogenerated electron and hole recombine. In order to overcome these challenges and drawbacks, a good number of modifications have been made on ZnO which extends its light absorption to the visible light region and thus enhances its photocatalytic capability. These modifications include the preparation of the nanoparticles and nanocomposites with organic materials, mono- and co-doping methods, and coupling with other semiconductors [13–15]. Non-metal doping does not lead to the formation of recombination centers. Unlike metal doping, it narrows the band gap by creating a new valence band through raising of the upper valence band. Hence, non-metal doping is preferred in introducing impurities to semiconductors which enhance their photocatalytic activity in the visible region [16]. Among the non-metals, nitrogen is the most promising candidate for doping due to its similarity with oxygen with regard to ionic radii and electronegativity [17].

Graphene, an allotrope of carbon with intriguing properties such as large specific surface area, unique electronic properties, excellent mechanical strength, and high transparency, has extraordinary applications in many areas including hydrogen production, capacitor, energy storage devices, nanoelectronics, sensors, and photocatalysis [18]. The oxidized form of graphene, graphene oxide (GO), can undergo exfoliation easily and forms a stable dispersion because of the presence of oxygen functionalities (located on their basal planes and epoxide and hydroxyl groups and also on their sheet edge, carboxyl and carbonyl functional groups) [19]. Large surface-to-volume ratio and two-dimensional structures of GO sheets may act as a good support material where functional nanomaterials can be loaded while the oxygen functionalities may act as a point of nucleation to hold the active materials. Recently, nanocomposites comprising of metal oxide/metal/GO have been reported and their respective potentiality as photocatalysts, biosensors, and capacitors [20–22] identified. Additionally, GO plays a very crucial part in influencing the performance of semiconductors in GO/semiconductors composite as a photocatalyst because of its electron transport abilities, adsorption capability, and large surface area [23]. Hence, we envisaged that doping ZnO with nitrogen would reduce the band gap of the semiconductor with minimum rearrangement in the crystal structure [24] while the presence of GO in the system would increase the adsorption rate of the semiconductor and also increase electron mobility at the interface. The synergetic effects of N and GO on ZnO are anticipated to improve the photocatalytic ability of ZnO by extending its light absorption to the visible region while inhibiting the rate at which electron and hole recombine at the semiconductor surface.

With respect to this study, we doped nitrogen into ZnO (N-ZnO) and immobilized the N-ZnO onto the GO surface via simple co-precipitation and wet chemical methods. The nanocomposites synthesized were further characterized in order to

analyze the effect the modifications of ZnO nanoparticle with nitrogen and GO will have on its photocatalytic capability. The photocatalytic ability of the photocatalyst was graded through the photodegradation of brilliant green dye in water.

Experimental procedures

Materials

The reagents and chemicals used (zinc acetate dihydrate; $Zn(O_2CCH_3)_2(H_2O)_2$, urea $CO(NH_2)_2$, sodium hydroxide (NaOH), brilliant green dye, graphite flakes, and potassium permanganate ($KMnO_4$)) were of analytical standard and procured from Sigma-Aldrich, Germany, and used as it purchased.

Synthesis of ZnO nanoparticle

To synthesize ZnO nanoparticle, 10 g of zinc precursor ($Zn(O_2CCH_3)_2(H_2O)_2$) was dissolved in deionized (DI) water (250 mL) under continuous magnetic stirring at 25 °C. Thereafter, 3 M NaOH under continuous and vigorous stirring was added slowly. The addition of NaOH stopped when the resultant reaction mixture gets to a pH of 12; the reaction continued for about 30 min with stirring to obtain a homogeneous mixture. The precipitate formed was washed using DI H_2O and C_2H_5OH simultaneously, dried for 12 h at a temperature of 50 °C, and calcined for 4 h at a temperature of 400 °C. The synthesized nanoparticle was stored as ZnO for further use.

Synthesis of N-doped-ZnO nanoparticles

Solvent-free reaction method was used in synthesizing N-ZnO nanoparticles (NPs) [25]. Un-calcined ZnO and urea were mixed and ground using agate mortar and pestle in a weight ratio of 1:2. Thereafter, the mixture was calcined for 4 h at a temperature of 400 °C. Thereafter, the mixture was taken out and allowed to stand for some time in order to cool, followed by grinding to get fine powder and stored for further use.

Graphene oxide synthesis

Graphene oxide synthesis was carried out using graphite flakes as a starting material by the modified “Hummers” method [26]. In a mixture of concentrated H_3PO_4 (40 mL) and concentrated H_2SO_4 (360 mL), a mixture of $KMnO_4$ (18 g) and graphite powder (3 g) was slowly added with continuous stirring. The resulting solution was allowed to heat at 50 °C with continuous and vigorous stirring for 12 h. Thereafter, the temperature of the reaction mixture was brought to 25 °C, and 30% H_2O_2 (about 5 mL) was added in drops with continued stirring. The resulting solution mixture was centrifuged for 10 min at 7500 rpm and washed using

deionized water, 30% HCl solution, and ethanol in succession followed by filtration using a Teflon membrane filter (1- μ pore size). The filtrate was finally coagulated with 200 mL of ether, filtered, and dried at 50 °C for overnight.

Synthesis of nitrogen-doped ZnO-immobilized GO composite

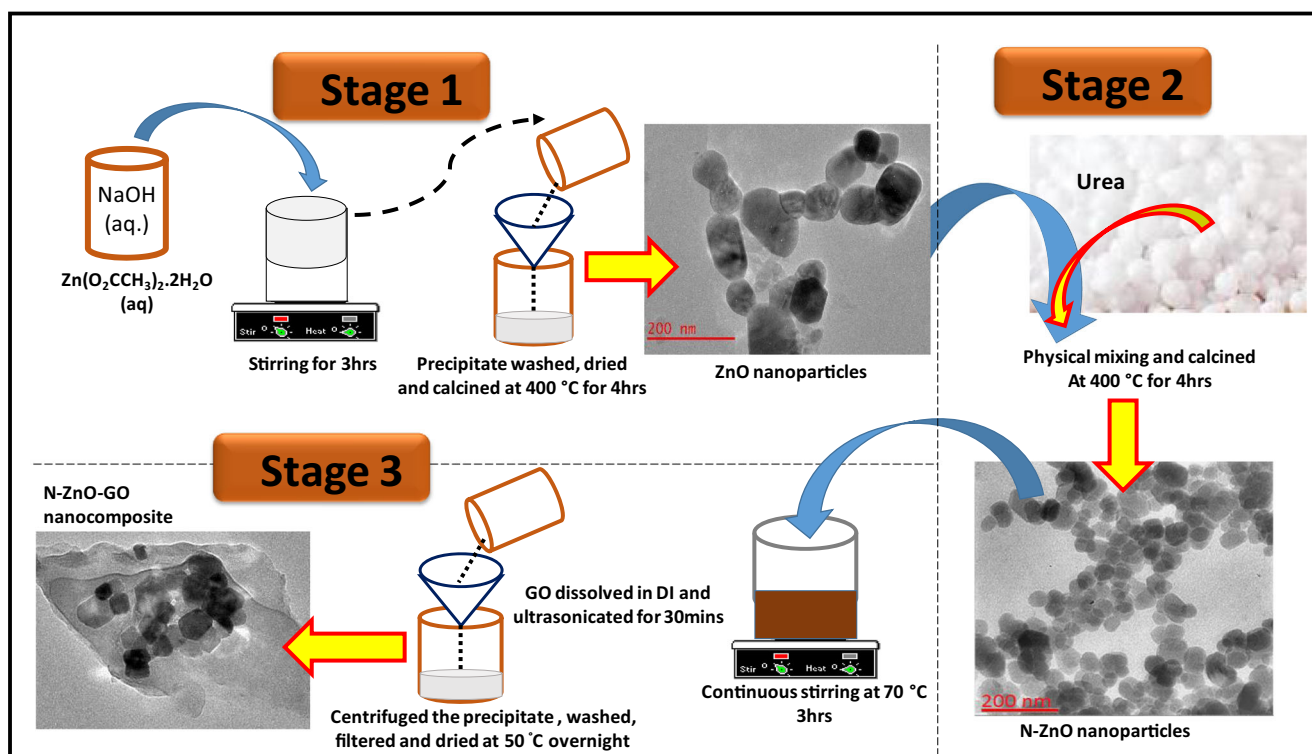
The N-ZnO-GO composite with 0.5 wt% of GO was prepared by using a wet chemical method similar to [27] starting with the dissolution of 0.04 g of GO in 60 mL of DI water and ultrasonicated for 30 min for exfoliation of GO. Thereafter, N-ZnO (0.4 g) was slowly added and the resulting solution was heated up to 3 h at a temperature of 70 °C under magnetic stirring. The reaction was cooled and centrifuged for 10 min at 7500 rpm followed by washing with DI water; a gray precipitate was obtained which was dried at 50 °C overnight and stored in desiccators for further use, labeled as NZGO-2. Other composites NZGO-1 representing 0.1 wt% of GO and NZGO-3 representing 1 wt% of GO were prepared using the same method by varying the GO ratio. A full schematic is provided in a three-stage preparation in Scheme 1.

Evaluation of photocatalytic activity

The photocatalytic performance of the nanocomposites synthesized was evaluated by making use of the photodegradation of BG dye under simulated visible light irradiation using 300-W Xe lamp (100 mW/cm²) with a 420-nm dichroic UV filter at 25 °C. Fifty milligrams of the photocatalyst in 100 mL of BG (20 ppm) was used for all the photodegradation experiments and the distance between the experimental setup and the light source was maintained at 10 cm in order to produce a light irradiation which is equivalent to 1 sun. Before exposure to the light, the dye and the photocatalyst adsorption-desorption equilibrium was obtained by stirring the mixture in the absence of light for 30 min. Thereafter, the mixture was exposed to light with continuous magnetic stirring and 3 mL of mixture withdrawn after 15-min intervals for a 90-min duration to monitor the concentration changes after light irradiation. The changes in the BG dye concentration in the solution before and after irradiation were determined using a UV–vis spectrophotometer (Shimadzu UV2450) at $\lambda = 623$ nm. The chemical oxygen demand (COD) of the dye solution before and after degradation was analyzed using the Spectroquant Pharo 300 and the COD percentage was calculated as per Eq. 1:

$$COD\% = \frac{COD_i - COD_f}{COD_i} \times 100 \quad (1)$$

where COD_i is the COD before (initial) degradation and COD_f is the COD after (final) degradation.



Scheme 1 Schematic diagram illustrating the three stages involved in the synthesis of N-ZnO-GO nanocomposite (GO = graphene oxide; N = nitrogen; ZnO = zinc oxide; DI = deionized water)

Characterization

The surface (external and internal) morphologies of the photocatalysts synthesized were analyzed on scanning electron microscopy (SEM) on a TESCAN (Vega 3 XMU) and TEM on a JEM-2100F, respectively. The elemental composition determination was done on energy-dispersive X-ray spectroscopy (EDX) which was coupled to the SEM. The crystallinity of the synthesized photocatalysts was analyzed by XRD at 40 kV, 30 mA with Cu K α radiation ($\lambda = 0.15406$) and K-beta filter. The presence of the functional groups in the synthesized photocatalyst was confirmed by using FTIR spectrometer (PerkinElmer FTIR spectrum-100). The photoluminescence (PL) spectra of the photocatalysts were generated using the PerkinElmer LS45 fluorescence spectrometer at room temperature with a Xe lamp and at 325-nm excitation wavelength while the optical properties of the photocatalysts were analyzed by using the UV–vis DRS (Shimadzu UV–2450) with barium sulfate as the reference.

Results and discussions

SEM, TEM, and EDS

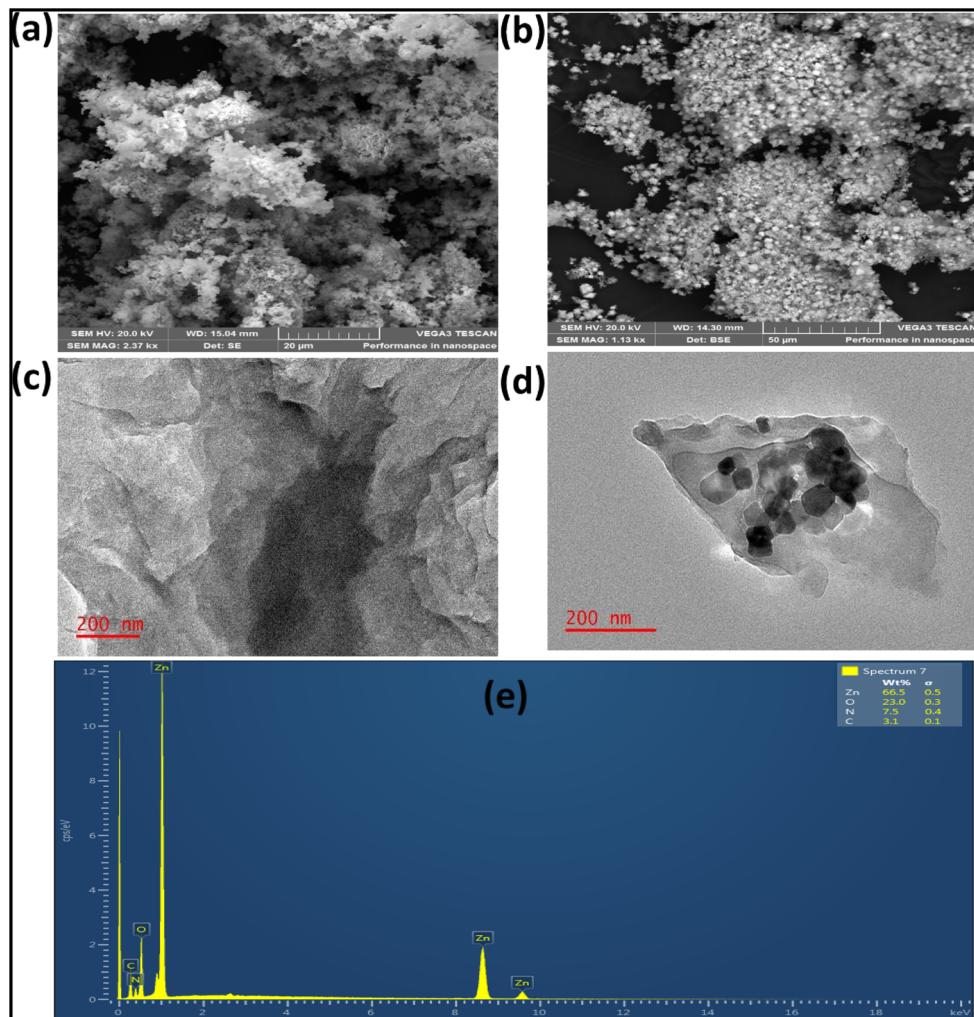
The SEM image of N-ZnO is depicted in Fig. 1a while Fig. 1b depicts the SEM image of N-ZnO-GO. N-ZnO nanoparticles

which have a relatively uniform size are densely packed on the surface of GO nanosheets illustrating the homogenous mixing of N-ZnO with the GO sheet. Figure 1c, d depicts the TEM image of sheet-like GO nanosheets and N-ZnO-GO nanocomposite, respectively. It is obvious from Fig. 1d that N-ZnO nanoparticles which have particle sizes between 15 and 35 nm are successfully immobilized over the surface of GO nanosheets. The coupling of N-ZnO onto the surface of GO nanosheets may be attributed to the presence of epoxide together with hydroxide groups on the GO sheets that act as sites of attachment for N-ZnO nanoparticles [28]. The elements present in the composite were analyzed using SEM-coupled EDS. Figure 1e showed the EDS spectrum of N-ZnO-GO materials to contain carbon, nitrogen, oxygen, and zinc element. The obtained results served as proof that the synthesized photocatalyst was uncontaminated with impurities during the synthesizing process.

FTIR, XRD, and BET analyses

The FTIR spectra of graphene oxide, NZGO-1, N-ZnO, and zinc oxide are illustrated in Fig. 2a. The characteristic bands of GO were identified at 3421, 1612, 1731, 1047, 1417, 1221, and 857 cm^{-1} , corresponding to OH stretchings, aromatics C=C stretchings, carbonyl CO stretching, alkoxy C–O stretching, carboxyl OH stretchings, and symmetrical and asymmetrical ether group stretching, respectively [29].

Fig. 1 SEM images for **a** N-ZnO and **b** NZGO-1, and TEM images of **c** GO and **d** NZGO-1 and **e** EDS spectrum of NZGO-1

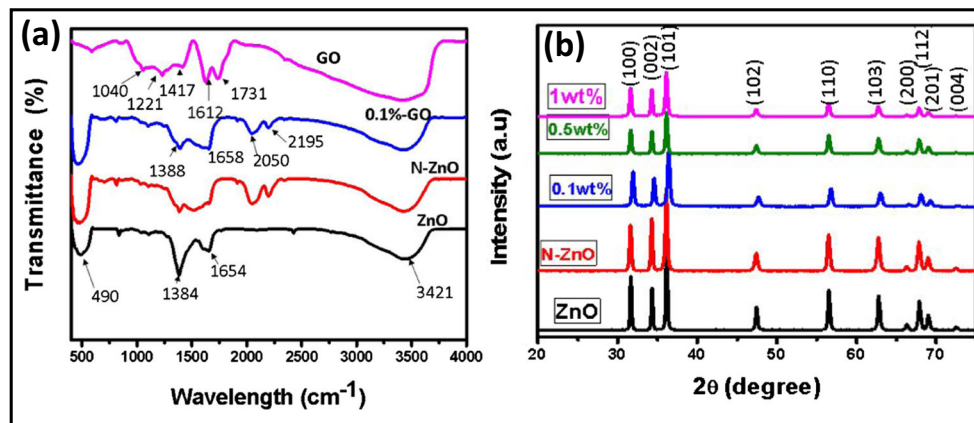


ZnO presence in the composite is confirmed by the typical vibration of Zn–O band elongation at 490 cm^{-1} . Additionally, the peaks observed around 1654 and 1388 cm^{-1} in the nano-composite are linked to the stretching vibrations of carboxylic of acetate groups (asymmetrical and symmetrical) attached to the ZnO [30] while the peak observed around 2050 cm^{-1} is related to the vibration of –OH groups [31]. Also, a blue shift

in the wavelength around the absorption peak 1657 cm^{-1} of the nanocomposite (NZGO-1) was observed compared to N-ZnO and ZnO and may be ascribed to complete exfoliation of GO nanosheets by N-ZnO. Hence, N-ZnO is successfully immobilized over the GO nanosheets.

XRD analysis gives an insight on the arrangement of atoms in its crystal structure. The XRD patterns of the

Fig. 2 **a** FTIR of GO, ZnO, N-ZnO, and NZGO-1 and **b** XRD pattern of the as-prepared photocatalysts



photocatalysts prepared (i.e., ZnO, N-ZnO, NZGO-1, NZGO-2, and NZGO-3) are illustrated in Fig. 2b. Observation from the figure shows that the diffraction peak patterns of N-ZnO, NZGO-1, NZGO-2, and NZGO-3 all match the hexagonal wurtzite structure of ZnO as depicted in ICDD: 04-008-8198 [32]. The similarity in the diffraction peaks of these as-prepared photocatalysts indicates that the modifications made on ZnO did not alter its structural pattern and orientation. Also, the absence of the typical GO diffraction peaks in the composite can be linked to its low diffraction intensity and its small amount which is an indication of complete exfoliation and dispersion of GO nanosheets in the nanocomposite [33].

The particle sizes of the nanocomposites were computed based on the diffraction peaks at 101 orientation plane using Debye–Scherrer's formula. While the lattice constants a (Eq. 2) and c (Eq. 3) were calculated based on 100 and 002 orientation planes, respectively, using modified Bragg's law [34], lattice constants

$$a(100) = \frac{\lambda}{\sqrt{3} * \sin\theta} \quad (2)$$

and

$$b(002) = \frac{\lambda}{\sin\theta} \quad (3)$$

The unit cell volume of the as-prepared photocatalyst was calculated using the following formula [35].

$$\sqrt{3} \times a^2 \times \frac{c}{2} \quad (4)$$

where a and c stand for the lattice constants of the cell.

As observed in Table 1, the crystalline size, the cell volume, and the lattice constants of ZnO decrease after modifications with N, presumed to link to the fact that N occupies interstitial positions in the ZnO crystal lattice.

The introduction of GO in the nanocomposite increased the specific surface area (S_{BET}) of ZnO from 4.4561 m² g⁻¹ in pristine ZnO to 22.123 m² g⁻¹ in 1%wt GO (N-ZnO-GO) as obtained from nitrogen adsorption/desorption process. The result is recorded in Table 1 and the observed changes in the surface area are linked to a higher surface area provided by graphene sheets (about 2630 m² g⁻¹). The largest increase in surface area was from the urea reaction to produce the N-ZnO (4.4 to 12.7 m² g⁻¹). The subsequent increases from adding GO are more incremental. The higher surface area is anticipated to facilitate adsorption of the

dye molecules from the dye solution and thus an enhanced photodegradation. Standard deviation of the surface area results was also calculated (Table 1). It can be found that the surface area results are consistent, varying only by a maximum of 4% thus making this result reliable.

UV–vis analysis

The higher the optical absorbance of a photocatalyst, in the visible region which spreads across over about 43% of the visible spectrum, the more effective it is for photocatalysis. Figure 3a depicts the UV–visible DRS of ZnO, N-ZnO, NZGO-1, NZGO-2, and NZGO-3, as measured using the UV–vis spectrophotometer set to a wavelength range between 200 and 800 nm. Figure 3a shows sharp absorption peak for ZnO around 388 nm which is a sign impurities suppressed ZnO nanoparticle and of good crystalline. As can be observed from the UV results, N-ZnO shows a slight red shift in wavelength compared to the pristine ZnO which can be attributed to the modifications made on the electronic levels of ZnO by incorporating nitrogen into its crystal structure. This observation may be related to the fact that there are more 2p π -electrons of nitrogen compared to the 2p π -electrons of those of the replaced oxygen in the lattice structure which decreases the band gap by creating another energy state between the VB of ZnO and its CB [34]. In comparison with the absorbance of ZnO and N-ZnO, the absorption of NZGO-1, NZGO-2, and NZGO-3 composites is more intensive in the whole visible light spectrum. A similar observation has also been documented in literature [36]. Again, Li et al. [37] noted a similar phenomenon where the modification of ZnO with GO improved the absorption of ZnO in the whole visible region. The increment in absorbance over the visible range may be credited to graphene oxide introduction in the N-ZnO-GO composite which not only increases the surface electrical charge of the oxides in the composite but also suppresses electron-hole formation process during irradiation [38]. Also, Fig. 3b which is a plot of Kubelka–Munk [39] function of energy against photon energy shows lowering of the band gap of the synthesized photocatalysts from 3.30 to 2.83 eV, affirming the reason for the increased absorbance in the visible region. Similar band gaps for ZnO (3.20 eV) and N-ZnO (2.98 eV) have been reported elsewhere in literature of [40, 41] and [25, 42], respectively. Hence, this increase in the absorbance of light intensity and range has the ability to increase the performance of the modified zinc oxide (with nitrogen and GO) compared to unmodified ZnO photocatalytically.

Table 1 Lattice parameters, cell volume, and crystallites of the as-prepared photocatalysts (standard deviation in parentheses)

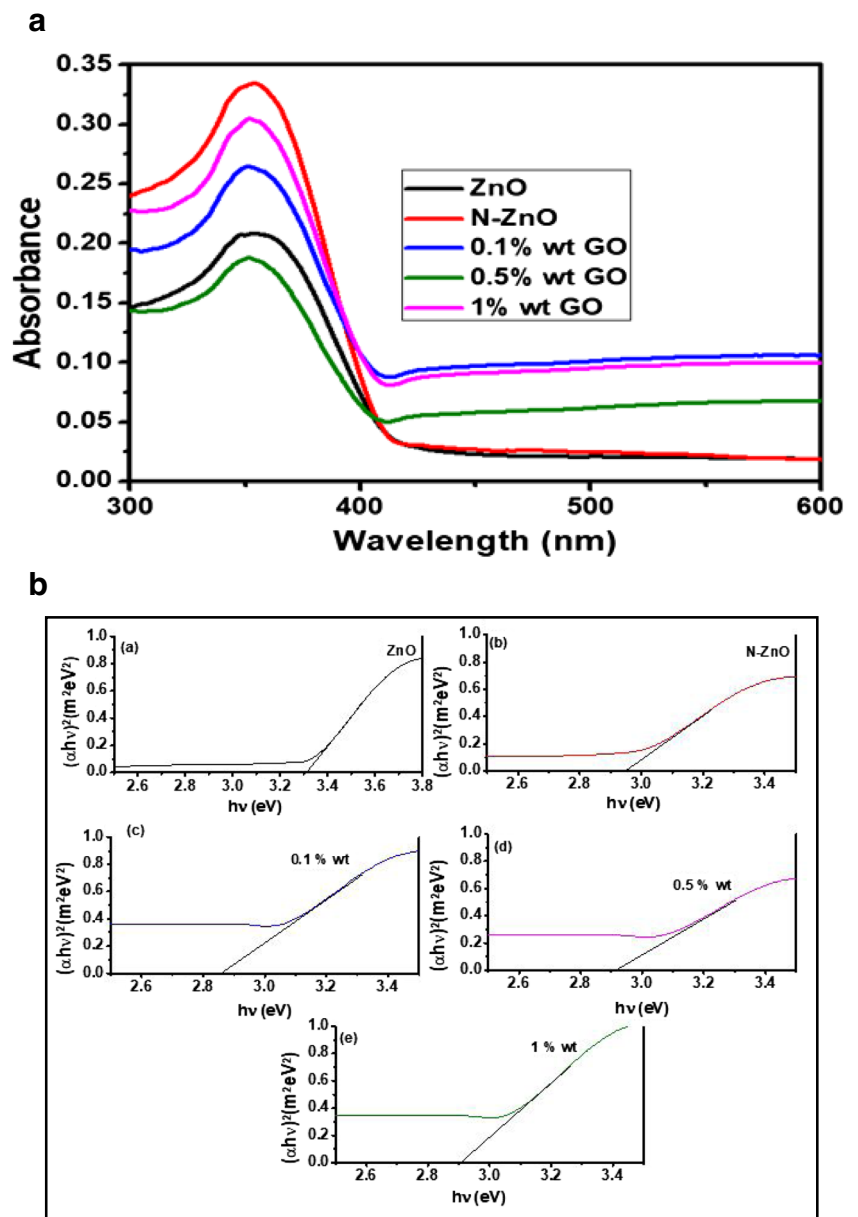
Name of sample	Lattice parameters in Å		Crystallite size (<i>d</i>) in nanometer (nm)	Cell volume in (Å) ³	<i>S</i> _{BET} in m ² g ⁻¹
	<i>a</i> = <i>b</i>	<i>C</i>			
ZnO	3.259	5.216	29.12	47.99	4.456 (2)
N-ZnO	3.256	5.216	26.67	47.92	12.681 (3)
NZGO-1	3.242	5.197	23.98	47.33	17.410 (1)
NZGO-2	3.259	5.220	29.65	48.05	20.325 (3)
NZGO-3	3.261	5.223	30.5	48.11	22.123 (4)

Photoluminescence spectra

One of the essential factors affecting the photocatalytic ability of a semiconductor used as a photocatalyst is the rate at which

photogenerated electron and hole recombine. The higher the recombination, the lower the photocatalytic activity of the respective semiconductor, due to less availability of carriers for generation of radicals which react and degrade organic

Fig. 3 a UV–vis DRS of the photocatalysts synthesized. b Tauc plots for the as-prepared photocatalysts



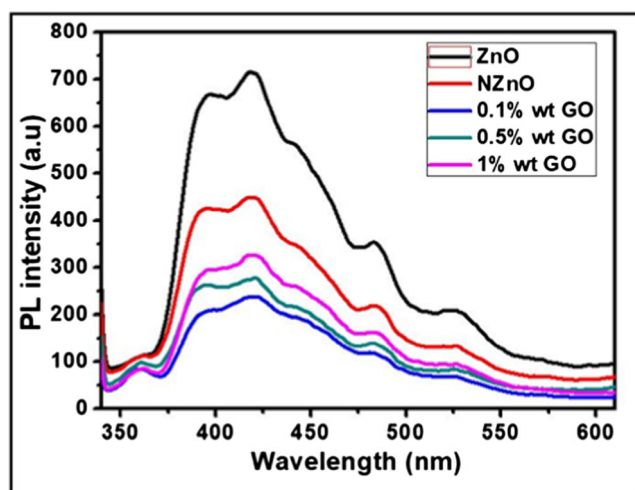


Fig. 4 Photoluminescence spectra of the as-prepared photocatalysts

dyes. Photoluminescence (PL) spectrum was used in this study to analyze the effect of nitrogen and GO in the electron-hole recombination rate of ZnO. Figure 4 depicts the PL spectra of ZnO, N-ZnO, NZGO-1, NZGO-2, and NZGO-3 measured using a set excitation wavelength of 325 nm. While a higher PL emission intensity suggests a faster electron-hole recombination rate, a lower PL emission intensity, on the other hand, indicates a slower electron-hole recombination rate. The peaks observed at 360 nm were linked to near band edge emission of ZnO; at 395 nm, it was linked to near UV emission which arises from the photogenerated electron-hole recombination, while the peak at 420 nm was linked to blue emission arising from the Zn interstitial donor level to Zn vacancy acceptor energy level; the peak at 482 nm is linked to blue-green emission and may be ascribed to the defects created by oxygen vacancies. In comparison, the PL spectrum intensities of ZnO and N-ZnO against the PL spectrum of the composite with 0.1%wt GO show the latter with the lowest intensity which is an indication of electron-hole recombination suppression and may be attributed to GO introduction in the composite. The lower intensity observed at the PL emission spectrum of the nanocomposite indicates an enhancement in the transfer charges taking place at the interface and thus suppressing the electron-hole recombination rate taking place at the defect sites, implying that the generation of photo-induced electrons in the CB of N-ZnO nanoparticles is conveyed rapidly to GO sheet. From PL spectrum results, NZGO-1 is expected to have a higher photocatalytic activity as compared to the respective ZnO and N-ZnO photocatalysts.

Photocatalytic degradation and mineralization of BG

The photocatalytic ability of the photocatalysts synthesized ZnO, N-ZnO, NZGO-1, NZGO-2, and NZGO-3; nanocomposites were investigated through the photodegradation of BG

dye under simulated visible light after 90 min of irradiation. Figure 5a is a representation of the UV–vis absorption spectrum of BG dye dissolved in water (starting dye concentration, 20 ppm in 100 mL of DI) with 0.05 g of the composite with NZGO-1 obtained at 25 °C after 90 min of irradiation time. As seen, the notable absorption peak of the dye at 623 nm decreases as the irradiation time increases and almost vanishes after 90 mins which is a promising indication that the concentration of BG decreases as the time at which it is exposed to irradiation increases.

The photodegradation efficiency of BG with the modified systems (i.e., N-ZnO, NZGO-1, NZGO-2, and NZGO-3) is much better than that of the unmodified ZnO as shown in Fig. 5b. The optimum degradation was observed with the nanocomposite containing 0.1%wt GO, while increasing the amount of GO beyond this was observed to inhibit the photocatalytic activity. Similar observations have been reported [29] with reasons related to the presence of excess GO in the system causing increased light irradiation absorption as well as scattering. This scattering effect leads to lower photocatalytic efficiency because only a small amount of light irradiation passes through the reaction mixture and thus a lower number of active sites of the catalyst are activated for photodegradation. The percentage removal of BG as illustrated in Fig. 5b was increased from 66 to 83, 88, 96, and 100% for the synthesized photocatalysts ZnO, N-ZnO, NZGO-1, NZGO-2, and NZGO-3, respectively, after 90 min of light irradiation. From the results above, it can be deduced that the increased photocatalytic capacity of the nanocomposites was because of the presence of GO in the system and the reduced band gap of the composites.

Introducing the GO to the nanocomposite makes it possible for more BG molecules to be adsorbed on the surface of the semiconductor as compared to the unmodified ZnO nanoparticles. In order to ascertain the adsorption abilities, the as-prepared photocatalyst was investigated at equilibrium and computed by using Eq. 5;

$$A_t = \frac{(C_0 - C_t)V}{m} \quad (5)$$

where A_t measured in milligrams per gram represents the amount of BG adsorbed per gram of the catalyst with time (t). C_0 and C_t are the concentration (initial) at $t=0$ and the concentration (final) of BG at time t in parts per million, respectively. V represents the volume of BG solution in milliliters and m stands for the mass of photocatalyst in grams. From the bar graph in Fig. 5d, it can be seen that the adsorption of BG increased from 20 to 26 mg g^{-1} , 28, 29, and 31 mg g^{-1} for the catalysts ZnO, N-ZnO, NZGO-1, NZGO-2, and NZGO-3, respectively. The increase in the adsorption ability of the

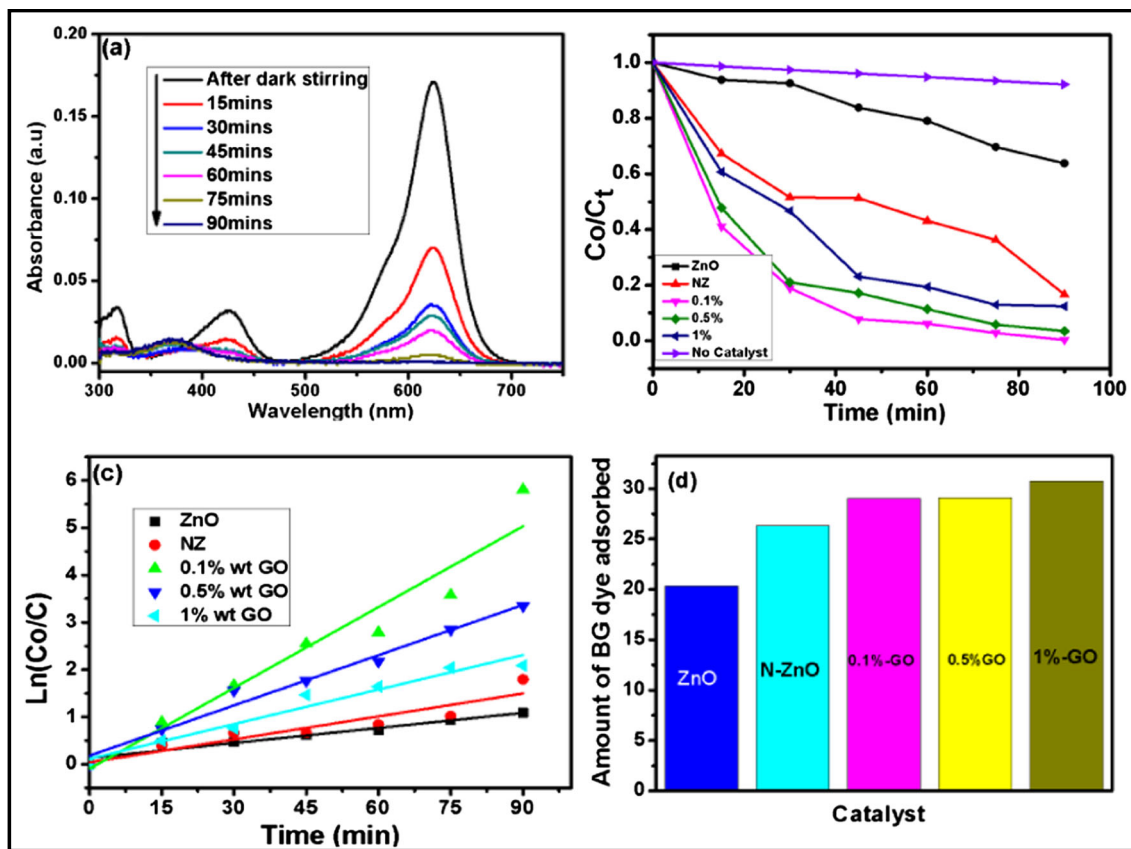


Fig. 5 **a** UV-absorption spectrum showing the photocatalytic degradation of BG under simulated visible light for NZGO-1, **b** illustration of the photodegradation of BG without a catalyst and with the as-prepared

photocatalysts, **c** the $\ln(C_0/C_t)$ versus time graph for the as-prepared photocatalysts, and **d** a bar graph showing the amount of BG in milligrams per gram absorbed after stirring in the dark for 15 min

composite on the introduction of GO may be related to a larger surface area of exposure and oxygen functionalities possessed by GO and the $\pi-\pi$ stacking interaction which exists between GO and BG which implies an increase in the surface electric charge of ZnO. Figure 5c shows that the photodegradation of BG under simulated visible light using the as-prepared photocatalysts obeyed Lagergren [43] pseudo first-order kinetics with respect to BG concentration:

$$\ln\left(\frac{C_0}{C_t}\right) = k \times t \tag{6}$$

where K is pseudo first-order rate constant and C_0 is the initial concentration at $t=0$, i.e., after stirring in the dark for 30 min. C_t stands for concentration at t =time. This is an indication that the dye is adsorbed onto the semiconductor surface occurs through. The rate constant of the composite (NZGO-1) is about five times greater than that of the unmodified ZnO as analyzed from Fig. 5c. This enhancement of the rate constant is observed because of the modifications made on ZnO using N and GO.

COD, which is a measure of the amount of dissolved oxygen gobbled by chemical oxidation of the organic matters in water, was used to investigate the extent of mineralization of the dye solution. With the optimum conditions, the COD obtained before degradation was 187 mg L^{-1} and was reduced to 37 mg L^{-1} after 90 min of irradiation. This corresponds to 80% degradation of BG.

Photodegradation kinetics and mechanism

Based on the fact that effluents from the industries can hardly be neutral, one important parameter not to be ignored in regard to wastewater treatment is the effect the pH of the dispersions has on the reaction rate. pH of the dissolution affects the charge on the semiconductor’s surface hence influencing how fast reactions take place on the semiconductor’s surface. Hence, pH effect on the photodegradation of BG was evaluated in this study and the results are displayed in Fig. 6a. Based on the issues of cost and the feasibility of carrying out pH adjustments at large scale, extreme pH values were not considered in this study; pH values in the range of 4–11 were used. From Fig. 6a, it is obvious that the photodegradation rate of BG increases as the pH increases up to a maximum pH of 9. Thereafter, a

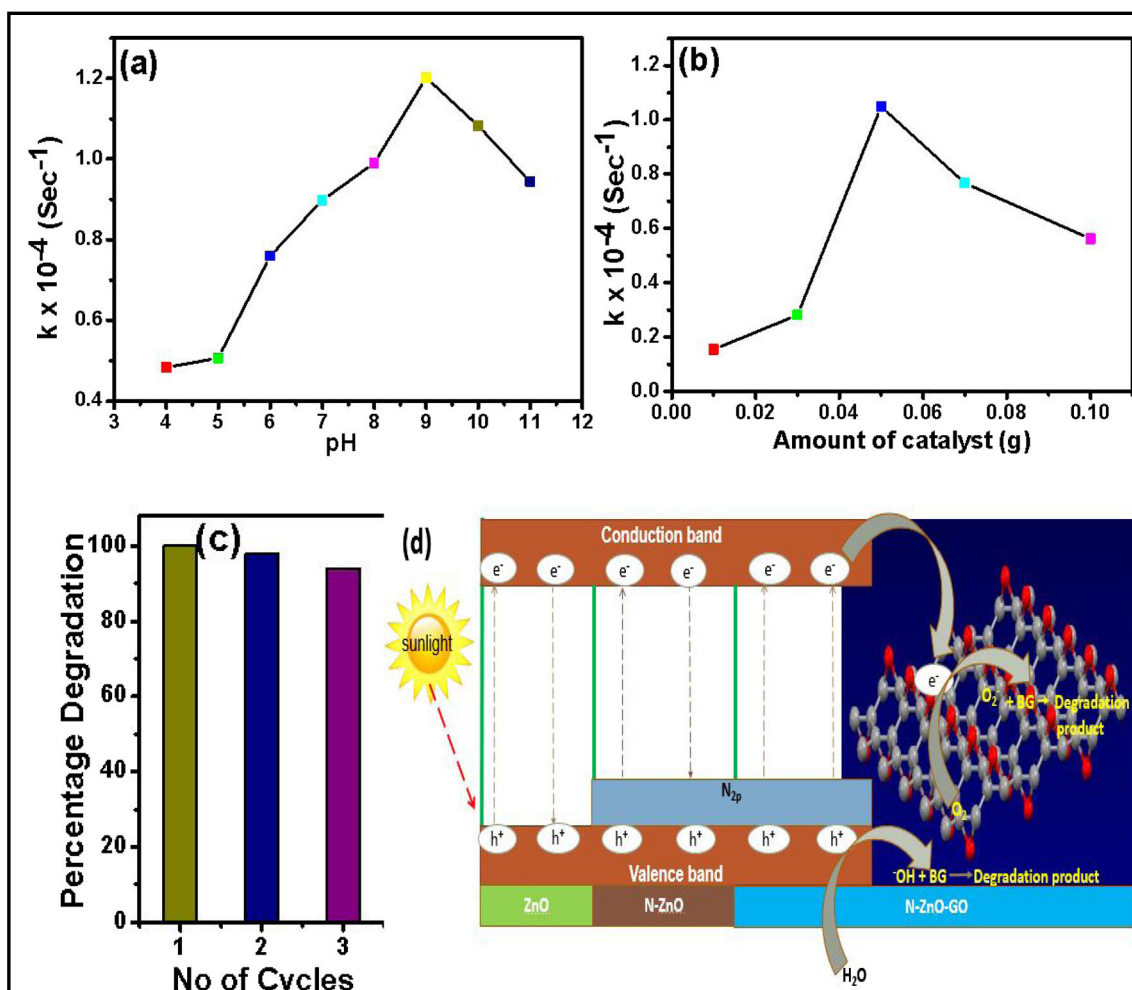


Fig. 6 **a** Effects of pH on the photodegradation of BG, **b** effect of photocatalyst dosage, **c** photostability of NZGO-1 after three times of use, and **d** photocatalytic mechanism

further increment in pH results in the retardation of the reaction rate. This observation may be ascribed to the fact that the surface of the semiconductor becomes negatively charged as pH increases making it easier for the cationic dye to be adsorbed onto the surface of the catalyst [44]. Since photodegradation process begins with adsorption of the dye, enhanced adsorption resulted in high degradation process. Also, increasing the pH leads to the generation of more active species in the system (e.g., $\cdot\text{OH}$ radicals) which results from the reaction between the photogenerated holes (h^+) of the semiconductor and the OH^- of the base [45]. Hence, an intimate interaction between the adsorbed dye and $\cdot\text{OH}$ radicals leads to a higher rate of degradation on increasing the pH value.

On further increasing the pH above the optimum value, the cationic dye changes into a neutral molecule hence making adsorption onto the surface of the photocatalyst difficult and therefore leading to the retardation in the rate of dye degradation. The effect of the amount of catalyst used in degradation of BG was studied by varying the amount of NZGO-1 from 0.01 to 0.1 g, while other parameters are kept constant (see

illustration in Fig. 6b). As can be observed from Fig. 6b, the rate of degradation of BG increased when the amount of the catalyst increases up to a maximum amount of 0.05 g. Thereafter, a further increase directly results in the retardation of the degradation rate.

This result may be ascribed to the fact that there are more numbers of active sites as well as active surface area of the catalyst when increasing the catalyst amount which may lead to more generation of superoxide and hydroxide radicals that enhance the photodegradation of BG. But on further increasing the catalyst amount above its optimum dose, there is a decrease in the photocatalyst's surface area (which would facilitate pollutant adsorption and light absorption) caused by particle–particle interaction (agglomeration). Also, the turbidity of the suspension increases resulting in less light penetration through the suspension and hence the decrease in the dye molecules' degradation rate.

The reusability of NZGO-1 in the photodegradation of BG was also investigated by using the photocatalyst three times consecutively in the photocatalytic experiment. As shown in

Table 2 Comparison of the results of some of the recent works based on the photodegradation of brilliant green dye in wastewater using different light sources with the present work

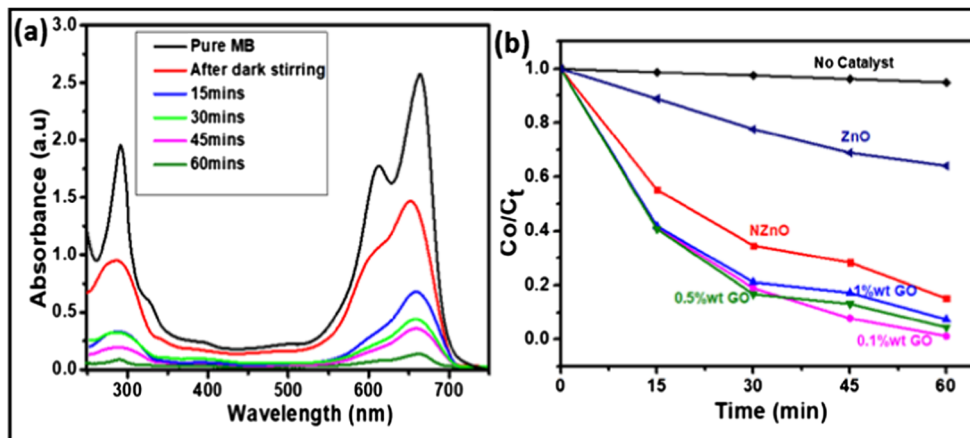
Photocatalyst	Conc (ppm)	Catalyst amount (mg/L)	Time (min)	Degradation (%)	Light source	Reference
Cu- and Ag-doped ZnO	10	1000	180	100	UV light	[48]
(ZnO-TiO ₂) -β-CD	20	2000	180	99	Visible light	[49]
H ₂ O ₂ -sensitized Bi ₂ WO ₆	10	1000	240	100	Visible light	[50]
H ₂ O ₂ -sensitized BiVO ₄	10	1000	90	≈ 100	Visible light	[51]
Mn-CDS _e QDS	10	300	90	86.5	Sunlight	[52]
Sr-TiO ₂	25	500	60	96	UV light	[53]
Sonophotocatalytic process in the presence of ZnO	15	2000	120	94.8	Immersed lamp sonophotocatalytic reactor	[54]
Ag ₈ SnS ₆	10	1250	90	92.31	Tungsten lamp	[55]
			300	73.43	Solar irradiation	
N-ZnO-GO	20	500	90	100	Visible light	Present work

the bar graph (Fig. 6c), 94% degradation of BG was still achieved after three cycles of photodegradation which illustrates the photocatalyst is photostable and can be reused during its application. The observed decrease in the photodegradation rate may be due to the loss of some photocatalyst during sample withdrawal for analysis, filtrations, and drying for reuse in the experiment. Figure 6d is a schematic illustration of the mechanism and charge transfers taking place during the photocatalytic activity of ZnO, N-ZnO, and NZGO-1 nanocomposites. As shown in Fig. 6e, on exposure to sunlight, there is the excitement of electrons to the CB of ZnO from its VB. With respect to the energy gap of unmodified ZnO, it is obvious that a greater amount of irradiation energy is needed to excite electrons to the CB from the VB of ZnO. Also, electron-hole recombination rate is high due to the fact that electrons are unstable in the CB and tend to drop back quickly to the VB. On introduction of nitrogen, as shown in Fig. 6e, there is a decrease in the energy gap caused by the formation of a new energy state which results from hybridizing O 2p and N 2p energy states. Although the band

gap was reduced, the recombination rate of electron hole was not greatly influenced and that is in agreement with the PL results in Fig. 5. On introduction of GO to the system as illustrated in Fig. 6e, the excited electrons are transferred to the GO nanosheets from the CB of ZnO. This transformation of excited electrons enhances charge separation and thus inhibits electron-hole recombination rate. Similar results have been previously reported [46, 47]. Superoxide radicals are produced from photogenerated electrons upon reaction with oxygen while the holes produce hydroxide radicals on reaction with water. These radicals degrade the dye molecules and organics in water into H₂O, CO₂, and non-toxic minerals. Therefore, the enhancement of the photocatalytic efficiency of NZGO-1 in the visible range of the visible spectrum is perhaps associated with the synergetic effects of N and GO in the synthesized nanocomposites.

The comparison of different photocatalysts used in the photodegradation of BG with the newly prepared photocatalyst presented in this work is displayed in Table 2. With respect to the light source, UV light forms only about 5%

Fig. 7 a UV-absorption spectrum showing the photocatalytic degradation of MB under simulated visible light for NZGO-1. b Photodegradation profile of MB using NZGO-1 photocatalysts



of the visible radiation while visible light covers up to 46% of the spectrum. Our newly synthesized photocatalyst used visible light in degradation of BG, hence a suitable candidate in terms of harvesting the more abundant visible radiation for photocatalysis. Also, referring to the length of degradation (in time), amount of catalyst used, dye concentration, and the degradation percentage, our newly prepared photocatalyst achieved 100% degradation of BG (20 ppm) dye within 90 min using as low as 500 mg L⁻¹ of the catalyst. These results infer that the as-prepared N-ZnO-GO is a viable photocatalyst in photodegradation of BG under visible light irradiation.

The tendency of the most efficient catalyst (NZGO-1) to mineralize other dyes was assessed by using it to degrade 20 ppm methylene blue (MB) dye at the optimum pH (pH 9) by following the same procedure as described in the “Evaluation of photocatalytic activity” section. The result indicates that the catalyst performed impressively well against the dye with 98% degradation efficiency (Fig. 7). Thus, the NZGO-1 nanocomposite is effective against the degradation of other dyes in water apart from brilliant green.

Conclusion

N-ZnO immobilized on GO nanosheets with different GO weight percentages (0.1, 0.5, and 1%) was successfully synthesized and characterized. The composites N-ZnO-GO, when compared to ZnO and N-ZnO, show an enhanced photocatalytic capability under visible region and may be ascribed to the combined effects of nitrogen and GO on ZnO nanoparticles which include increased adsorption rate, reduced band gap, and the slower rate at which electron and hole recombine. The photodegradation rate of BG by the composite was observed to be dependent on the amount of GO and the optimum degradation was obtained with the composite having NZGO-1. At higher GO content, there is lighter scattering than penetration through the solution which then decreases the photocatalytic ability of the composites containing NZGO-2 and NZGO-3. Also, a higher amount of GO in the composite affects the crystallite size of ZnO. The results also showed that the degradation of BG using NZGO-1 with an optimum amount of 0.05 mg occurs faster in basic medium (pH 9) compared to that in acidic medium. Photostability test of NZGO-1 analyzed after three cycles of exposure gave 94% degradation of BG which implies that the composite is also highly stable and can be recovered and reused. From the results, it can be concluded that N-ZnO-GO is an appropriate photocatalyst for efficient photodegradation and mineralization of BG dye in water and future work in this project will investigate photodegradation of other forms of organic dyes in wastewater.

Acknowledgements The authors express their gratitude to the Faculty of Science, University of Johannesburg and National Research Foundation (NRF) for their support financially while executing this research.

Compliance with ethical standards

Conflict of interest The authors declare that they have no conflict of interest.

References

1. Pathania D, Gupta D, Ala'a H, Sharma G, Kumar A, Naushad M, Ahamad T, Alshehri SM (2016) Photocatalytic degradation of highly toxic dyes using chitosan-g-poly (acrylamide)/ZnS in presence of solar irradiation. *J Photochem Photobiol A Chem* 329:61–68
2. <http://science.howstuffworks.com/environmental/earth/geophysics/h2o1.htm>. Accessed May 2017
3. Turabik M, Gozmen B (2013) Removal of basic textile dyes in single and multi-dye solutions by adsorption: statistical optimization and equilibrium isotherm studies. *CLEAN—Soil, Air, Water* 41: 1080–1092
4. Gupta V (2009) Application of low-cost adsorbents for dye removal—a review. *J Environ Manage* 90:2313–2342
5. Börnick H, Schmidt TC (2006) Amines. in *Organic pollutants in the water cycle: properties, occurrence, analysis and environmental relevance of polar compounds*. 181–209
6. Suteu D, Zaharia C, Bilba D, Muresan R, Popescu A, Muresan A (2009) Decolorization waste waters from the textile industry—physical methods, chemical methods. *Ind Text* 60:254–263
7. Yue Z, Mangun C, Economy J, Kemme P, Cropek D, Maloney S (2001) Removal of chemical contaminants from water to below USEPA MCL using fiber glass supported activated carbon filters. *Environ Sci Technol* 35:2844–2848
8. Mamba B, Krause R, Matsebula B, Haarhoff J (2009) Monitoring natural organic matter and disinfection by-products at different stages in two South African water treatment plants. *Water SA* 35: 121–127
9. Kaushik P, Malik A (2009) Fungal dye decolourization: recent advances and future potential. *Environ Int* 35:127–141
10. Ohtani B (2010) Photocatalysis A to Z—what we know and what we do not know in a scientific sense. *J Photochem Photobiol C: Photochem Rev* 11:157–178
11. Zou Y, Gong Y, Lin B, Mellott NP (2016) Photodegradation of methylene blue in the visible spectrum: an efficient W⁶⁺ ion doped anatase titania photocatalyst via a solvothermal method. *Vacuum* 126:63–69
12. Tian C, Zhang Q, Wu A, Jiang M, Liang Z, Jiang B, Fu H (2012) Cost-effective large-scale synthesis of ZnO photocatalyst with excellent performance for dye photodegradation. *Chem Commun* 48: 2858–2860
13. Anku WW Opong SOB, Shukla SK, Govender PP (2016) Synthesis and characterisation of neodymium doped-zinc oxide-graphene oxide nanocomposite as a highly efficient photocatalyst for enhanced degradation of indigo carmine in water under simulated solar light. *Res Chem Intermed* 481–501
14. Mzoughi M, Anku WW Opong SO-B, Shukla SK, Agorku ES, Govender PP (2016) Neodymium doped ZrO₂-graphene oxide nanocomposites: a promising photocatalyst for photodegradation of eosin Y dye. *Adv Mater Lett* 7:100–150
15. Ma R, Wang X, Huang J, Song J, Zhang J, Wang X (2017) Photocatalytic degradation of salicylic acid with magnetic activated carbon-supported F-N codoped TiO₂ under visible light. *Vacuum* 141:157–165
16. Samadi M, Zirak M, Naseri A, Khorashadizade E, Moshfegh AZ (2016) Recent progress on doped ZnO nanostructures for visible-light photocatalysis. *Thin Solid Films* 605:2–19

17. Qin H, Li W, Xia Y, He T (2011) Photocatalytic activity of heterostructures based on ZnO and N-doped ZnO. *ACS Appl Mater Interfaces* 3:3152–3156
18. Allen Matthew J, Tung Vincent C, Kaner Richard B (2010) Honeycomb carbon a review of graphene. *Chem Rev* 110:132–145
19. Zhang N, Yang M-Q, Tang Z-R, Xu Y-J (2013) Toward improving the graphene–semiconductor composite photoactivity via the addition of metal ions as generic interfacial mediator. *ACS Nano* 8:623–633
20. Khoa NT, Kim SW, Yoo D-H, Cho S, Kim EJ, Hahn SH (2015) Fabrication of Au/graphene-wrapped ZnO-nanoparticle-assembled hollow spheres with effective photoinduced charge transfer for photocatalysis. *ACS Appl Mater Interfaces* 7:3524–3531
21. Rahman MM, Marwani H, Algethami F, Asiri A (2017) Xanthine sensor development based on ZnO-CNT, ZnO-CB, ZnO-GO and ZnO nanoparticles: an electrochemical approach. *New J Chem* 41: 6262–6271
22. Mahlangu O, Nackaerts R, Mamba B, Verliefdede A (2017) Development of hydrophilic GO-ZnO/PES membranes for treatment of pharmaceutical wastewater. *Water Sci Technol* 76:501–514
23. Rabieh S, Nassimi K, Bagheri M (2016) Synthesis of hierarchical ZnO–reduced graphene oxide nanocomposites with enhanced adsorption–photocatalytic performance. *Mater Lett* 162:28–31
24. Lee KM, Lai CW, Ngai KS, Juan JC (2016) Recent developments of zinc oxide based photocatalyst in water treatment technology: a review. *Water Res* 88:428–448
25. Kumar S, Baruah A, Tonda S, Kumar B, Shanker V, Sreedhar B (2014) Cost-effective and eco-friendly synthesis of novel and stable N-doped ZnO/gC₃N₄ core–shell nanoplates with excellent visible-light responsive photocatalysis. *Nano* 6:4830–4842
26. Marcano DC, Kosynkin DV, Berlin JM, Sinitskii A, Sun Z, Slesarev A, Alemayehu LB, Lu W, Tour JM (2010) Improved synthesis of graphene oxide. *ACS Nano* 4:4806–4814
27. He G, Huang J, Liu W, Wang X, Chen H, Sun X (2012) ZnO–Bi₂O₃/graphene oxide photocatalyst with high photocatalytic performance under visible light. *Mater Technol* 27:278–283
28. Park S, Lee K-S, Bozoklu G, Cai W, Nguyen ST, Ruoff RS (2008) Graphene oxide papers modified by divalent ions—enhancing mechanical properties via chemical cross-linking. *ACS Nano* 2:572–578
29. Huang K, Li Y, Lin S, Liang C, Wang H, Ye C, Wang Y, Zhang R, Fan D, Yang H (2014) A facile route to reduced graphene oxide–zinc oxide nanorod composites with enhanced photocatalytic activity. *Powder Technol* 257:113–119
30. Segala K, Dutra RL, Franco CV, Pereira AS, Trindade T (2010) In situ and ex situ preparations of ZnO/poly- $\{trans-[RuCl_2(vpy)_4]/styrene\}$ nanocomposites. *J Braz Chem Soc* 21:1986–1991
31. Hosseini SA, Babaei S (2017) Graphene oxide/zinc oxide (GO/ZnO) nanocomposite as a superior photocatalyst for degradation of methylene blue (MB)-process modeling by response surface methodology (RSM). *J Braz Chem Soc* 28:299–307
32. Albertsson J, Abrahams S, Kvik Å (1989) Atomic displacement, anharmonic thermal vibration, expansivity and pyroelectric coefficient thermal dependences in ZnO. *Acta Crystallogr Sect B: Struct Sci* 45:34–40
33. Gao P, Liu J, Sun DD, Ng W (2013) Graphene oxide–CdS composite with high photocatalytic degradation and disinfection activities under visible light irradiation. *J Hazard Mater* 250:412–420
34. Welderfael T, Yadav O, Tadesse AM, Kaushal J (2013) Synthesis, characterization and photocatalytic activities of Ag-N-codoped ZnO nanoparticles for degradation of methyl red. *Bull Chem Soc Ethiop* 27:221–232
35. Ullah Z, Atiq S, Naseem S (2013) Indexing the diffraction patterns and investigating the crystal structure of Pb-doped strontium ferrites. *J Sci Res* 5:235–244
36. Min Y, Zhang K, Zhao W, Zheng F, Chen Y, Zhang Y (2012) Enhanced chemical interaction between TiO₂ and graphene oxide for photocatalytic decolorization of methylene blue. *Chem Eng J* 193:203–210
37. Li B, Liu T, Wang Y, Wang Z (2012) ZnO/graphene-oxide nanocomposite with remarkably enhanced visible-light-driven photocatalytic performance. *J Colloid Interface Sci* 377:114–121
38. Xu T, Zhang L, Cheng H, Zhu Y (2011) Significantly enhanced photocatalytic performance of ZnO via graphene hybridization and the mechanism study. *Appl Catal B Environ* 101:382–387
39. Tauc J, Abeles F (1972) Optical properties of solids. North-Holland, Amsterdam
40. Baitha PK, Manam J (2015) Structural and spectroscopic diagnosis of ZnO/SnO₂ nanocomposite influenced by Eu³⁺. *J Rare Earths* 33: 805–813
41. Sawant SY, Cho MH (2015) Facile electrochemical assisted synthesis of ZnO/graphene nanosheets with enhanced photocatalytic activity. *RSC Adv* 5:97788–97797
42. Shet S, Ahn K-S, Deutsch T, Wang H, Ravindra N, Yan Y, Turner J, Al-Jassim M (2010) Synthesis and characterization of band gap-reduced ZnO: N and ZnO:(Al, N) films for photoelectrochemical water splitting. *J Mater Res* 25:69–75
43. Yuh-Shan H (2004) Citation review of Lagergren kinetic rate equation on adsorption reactions. *Scientometrics* 59:171–177
44. Kumar A, Kumar A, Sharma G, Ala'a H, Naushad M, Ghfar AA, Stadler FJ (2018) Quaternary magnetic BiOCl/g-C₃N₄/Cu₂O/Fe₃O₄ nano-junction for visible light and solar powered degradation of sulfamethoxazole from aqueous environment. *Chem Eng J* 334:462–478
45. Moussa H, Giroto E, Mozet K, Alem H, Medjahdi G, Schneider R (2016) ZnO rods/reduced graphene oxide composites prepared via a solvothermal reaction for efficient sunlight-driven photocatalysis. *Appl Catal B Environ* 185:11–21
46. Huo P, Zhou M, Tang Y, Liu X, Ma C, Yu L, Yan Y (2016) Incorporation of N–ZnO/CdS/graphene oxide composite photocatalyst for enhanced photocatalytic activity under visible light. *J Alloys Compd* 670:198–209
47. Zhang W, Zou X (2016) Synthesis, characterization and photocatalytic activity of reduced graphene oxide-Ce/ZnO composites. *Korean Chem Eng Res(화학공학)* 54:127–134
48. Gnanaprakasam A, Sivakumar V, Thirumarimurugan M (2016) A study on Cu and Ag doped ZnO nanoparticles for the photocatalytic degradation of brilliant green dye: synthesis and characterization. *Water Sci Technol* 74:1426–1435
49. Velusamy P, Lakshmi G (2017) Improved photocatalytic performance of (ZnO/TiO₂)- β -CD on decolorization of brilliant green dye under UV light irradiation. *India J Chem* 56A:43–49
50. Deepthi K, Murthy TN, Umabala A, Rao AP ISSN 0975-413X CODEN (USA): PCHHAX
51. Umabala A, Suresh P, Rao AP (2016) Effective visible light photocatalytic degradation of brilliant green using H₂O₂ sensitized BiVO₄. *Der Pharma Chemica* 8:61–66
52. Thirugnanam N, Govindarajan D (2016) Photodegradation studies of Mn doped CDSE Qds on brilliant green dye under sunlight irradiation. *Int J Recent Sci Res* 7:13377–13382
53. Sood S, Umar A, Kumar Mehta S, Sinha ASK, Kumar Kansal S (2015) Efficient photocatalytic degradation of brilliant green using Sr-doped TiO₂ nanoparticles. *Ceram Int* 41 (3533–3540)
54. Gole VL, Priya A, Danao SP (2017) Decolorization of brilliant green dye using immersed lamp sonophotocatalytic reactor. *Appl Water Sci* 7:4237–4245
55. Shambharkar BH, Chowdhury AP (2016) Ethylene glycol mediated synthesis of Ag₈Sn₆ nanoparticles and their exploitation in the degradation of eosin yellow and brilliant green. *RSC Adv* 6:10513–10519